SCIENTIA CUM INDUSTRIA(SCI. CUM IND.), V. 3, N. 2, PP. 59 — 66, 2015

The effect of counterpart material on the sliding wear of TiAlN coatings deposited by reactive cathodic pulverization

Michell Felipe Cano Ordoñez*†, Johan Steeven Restrepo Paruma*, Federico sequeda Osorio† and María Cristina Moré Farias*

Abstract

This work aims to study the effect of the counterpart materials (100Cr6, Al_2O_3 and WC-Co) on the tribological properties of TiAlN thin films deposited on AISI H13 steel substrate by reactive magnetron co-sputtering. The structural characterization of the TiAlN films, performed by X-ray diffraction, showed (220) textured fcc crystalline structure. The values of hardness and elastic modulus obtained by nanoindentation were 27 GPa and 420 GPa, respectively, which resulted in films with a relatively high resistance to plastic deformation. Ball-on-disk sliding tests were performed using normal loads of 1 N and 3 N, and 0.10 m/s of tangential velocity. The wear coefficient of the films was determined by measuring the worn area using profilometry every 1000 cycles. The mechanical properties and the chemical stability of the counterpart material, debris formation and the contact stress influences the friction and the wear behavior of the studied tribosystems. Increasing the hardness of the counterpart decreases the coefficient of friction (COF) due to lower counterpart material transference and tribofilm formation, which is able to support the contact pressure. High shear stress concentration at the coating/substrate interface was reported for higher load promoting failure of the film-substrate system for all tribopairs.

Keywords
TiAlN coatings, friction, wear, counterpart

I. Introduction

Industrial developments in the last years have generated demands for materials' technologies focused on surface improvements on industrial parts. Transition metals hard coatings have been used to enhance surface properties such as wear and corrosion resistance. Carbides, nitrides and combinations of them have been used intensively in industry [1]–[3]. Titanium nitride films deposited by plasma enhanced physical vapor deposition (PEPVD) have been used in a variety of industrial applications such as cutting tools, decorating, thermal barriers in electronic devices, corrosive inhibitor pieces and joint implants [4]–[6]. Although the lifetime of cutting tools has been significantly increased, TiN coatings have some limitations due to their high instability and rapid oxidation above 550C^{o} [7], [8]. To solve these problems, other chemical elements can be added to stabilize the compound. The aluminum is frequently used to form titanium-aluminum nitride (Ti-Al)N [9]–[12]. (Ti-Al)N thin films deposited by PVD have high hardness at elevated temperatures (800^{o}C) and improved performance in cutting operations at higher velocities compared to TiN [13], [14].

The higher oxidation resistance of the TiAlN coatings has been previously verified and this fact was attributed to the formation of an adherent, stable, passive, double-layer oxide, which is formed on the material's surface by titanium and aluminum diffusion [15]–[17]. This double-layer oxide reduces further oxidation by oxygen saturation and diffusion inhibition. Additionally, aluminum oxide on the surface can act as solid lubricant films when it works at high temperatures [17].

Origins of friction and wear of materials are found in the contact mechanisms produced at microscale, which describe stress and strain formation at asperities contacts, crack nucleation and propagation, material loss and debris formation [18]. The involved wear mechanisms of hard coatings are also related to the chemical nature of the counterface material in such a manner that in metallic and ceramic counterfaces, coating wear mechanisms are dominated by tribochemical reactions. In zirconia-steel (ceramic-metallic) counterpairs, wear rate is determined by chemical dissolution of the ceramic into the iron oxide [19]. On the other hand, for ceramic-ceramic counterpairs, wear coefficient can be dominated by surface hydration promoting low friction-debris formation [20]. Damages of the contacting surfaces induce the formation of a third body, which can be composed of oxide layers or particles detached from both the body and the counterpart. A fraction of the wear particles generated during sliding remains in the contact between the two surfaces and is transformed by further sliding process (plastic deformation, micro-welding, ploughing and cutting), modifying contact stresses and, in some cases, forming protective layers called tribofilms [15].

In this work, the effect of counterface material in tribological properties of TiAlN thin films deposited by DC magnetron sputtering was studied by evaluating surface roughness profiles and mechanical properties of the thin films, the coefficient of friction and wear coefficient of the contacting pairs, as well as the profile, the chemical composition and the morphology of the wear tracks.

* Laboratorio de Recubrimientos Duros y Aplicaciones Industriales (RDAI), Universidad del Valle, Cali – Colombia; †. Programa de Pós-Graduação em Engenharia e Ciência dos Materiais (PGMAT), Universidade de Caxias do Sul – Brazil.

michaelfkn@gmail.com,johansrestrepo@gmail.com,fsequeda@yahoo.com, mcmfarias@ucs.br

Data de envio:09/09/2015
Data de aceite:25/10/2015

http://dx.doi.org/10.18226/23185279.v3iss2p59

II. Experimental Procedure

TiAlN thin films were deposited using DC reactive magnetron co-sputtering in an AJA International ATC 1500. Ti and Al (99,99% purity) of 5.08 cm diameter targets were used with a 10 and 5 W/cm^2 power density respectively. Prior to deposition, 15 min plasma cleaning was conducted to eliminate residual contamination of the substrate and the cathode surface. The coatings were prepared at a fixed sputtering pressure of 0.7 Pa. The flow rates of N_2 and Ar gases were controlled separately by mass flow controllers. The effect of deposition parameters in the coatings properties were studied in previous works [21], [22]. Table I shows the specific deposition parameters used in this study.

TABLE I: Deposition parameters for TiAlN thin films

Substrate	Temperature (°C)	Bias voltage (V)	N_2(sccm)/ Ar(sccm) ratio	Work pressure (Pa)
H13	50	-100	0.1/10	0.7

In order to identify the phases and crystalline structure of the deposited films, X-ray diffraction (XRD) analyses were performed, in a Bruker D8 advance diffractometer, with a CuKα (λ=1.5406Å) source, θ-2θ geometry ranging from 20° to 80° with the glazing angle of 1°. Morphological and elemental chemical analyses were performed on the unworn surfaces and wear tracks using JEOL JSM 6490 LV SEM/EDS systems.

The roughness (arithmetic average height, Ra) average values and the wear track profiles were obtained in XP-2 Ambios technologies profilometer, with a resolution 10Å to 100 μm. The value of the Ra roughness corresponded to the average of 10 measurements.

Adhesion of the deposited thin films to the substrate was evaluated by means of scratch tests with Micro Test Instruments, where a diamond stylus with conical geometry and spherical tip (Rockwell indenter) is moved across the coating surface producing a scratch track. Several tracks were produced with an increasing normal load until film failure, which was associated with a sudden increase in the scratch coefficient of friction (SCF) versus normal load plot [21]. The normal load corresponding to SCF change (a step, or a change in slope) was considered as the critical scratch load (L_C), which was taken as a coating-substrate adhesive failure indicator. Table II shows the parameters used in the scratch tests. Hardness (H) and elastic modulus (E) were obtained by nanoindentation tests using a Nanovea Microphotonics Nanoindentation Equipment, with a diamond Berkovich indentator, coupled to an IBIS Fischer-Cripps Labs nanoindentation head. The H and E values of the TiAlN films were calculated from indentation load-displacement data taken from depths below 10% of total film thickness and by applying the Oliver-Pharr method, which was also previously used to calibrate the indenter area function and the frame compliance of the instrument (35 x 10^{-5} μm(mN)$^{-1}$) [23], [24]. The average values of twenty indentations were reported. The H^3/E^2 ratio was also calculated and used as an indicator of the resistance to plastic deformation of the film [25].

TABLE II: Scratch adhesion test condition for TiAlN-substrate

Load (N)	Loading rate (N.s^{-1})	Total scratch length (mm)	Displacement speed (mm.s^{-1})
0-90	1	6	4.5

A CSEM Instruments ball-on-disk type tribometer was used to analyze the coefficient of friction (COF) evolution for different counterpairs materials, using balls of 6 mm in diameter made of 100Cr6 (AISI 52100), alumina (Al_2O_3) and tungsten carbide (WC). Table III shows the parameters used in the sliding wear tests.

TABLE III: Scratch adhesion test condition for TiAlN-substrate

Load (N)	Tangential velocity (m.s^{-1})	Number of cycles	Relative humidity (%)
1 3	0.10	4000	75

Tribox 2.9 software was used to calculate the specific wear rate or wear coefficient (k) from the Archard equation (Eq. 1) [26], where (V) is the wear volume, calculated using profilometry measurements of the wear scar. W is the normal load and L is the sliding distance.

$$k = \frac{V}{WL} \tag{1}$$

The Hertzian maximum pressure ($_{pmax}$) was also calculated using Eqs. 2-5, where W is the normal load; a is the radius of the contact area; R' is the reduced radius of curvature; E' is the reduced Young's modulus; R_b is the ball radius; ν_b and ν_f are the Poisson's ratios of the ball and film, respectively; E_b and E_f are the Young's moduli of the ball and film, respectively. The film Young's modulus used in Eq. 5 was that obtained in nanoindentation tests and, the Poisson's ratio was taken from literature [27].

A Nanovea stereoscopy (x10) coupled to the displacement control table was used to observe worn surface characteristics every 1000 cycles.

$$p_{max} = \frac{3W}{2\pi a^2} \tag{2}$$

$$a = \left(\frac{3WR'}{E'}\right)^{1/3} \tag{3}$$

$$\frac{1}{R'} = \frac{2}{R_b} \tag{4}$$

$$\frac{1}{E'} = \frac{1}{2}\left[\left(\frac{1-\nu_b^2}{E_b} + \frac{1-\nu_f^2}{E_f}\right)\right] \tag{5}$$

III. Results and Discussion

A. Coating characteristics

The analysis of XRD patterns of TiAlN films showed a TiAlN structure like a face centered cubic fcc-NaCl (Figure 1). The structure is highly textured in the (220) crystallographic orientation, besides being characterized by the presence of (111) and (311) diffraction peaks. These results indicated that a solid solution between Ti and Al is formed, with aluminum

atoms in the crystalline structure of cubic-TiN generating an interstitial nitride [28][28]. The absence of (200) peak is related to the low N_2/Ar ratio used in this work. For higher N_2/Ar ratios, the aluminum nitriding produces separation of h-AlN(101) and c-TiAlN(200) phases and also inhibits TiAlN (220) growth [28], [29].

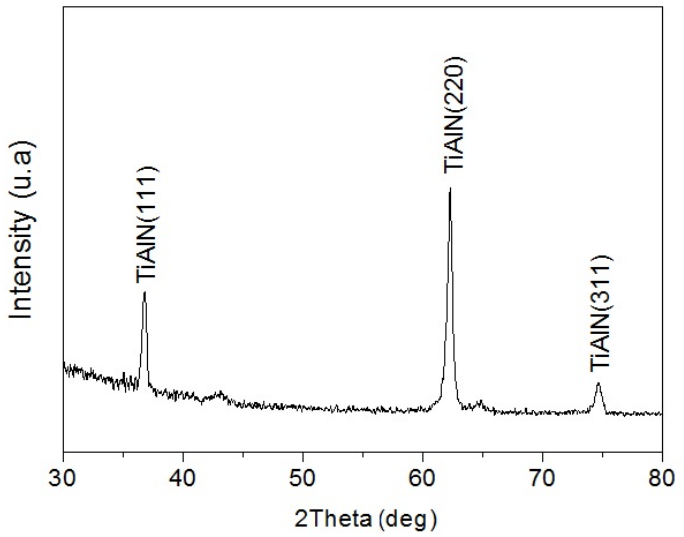

Fig. 1: XRD pattern of TiAlN thin films.

Table IV shows the thickness, deposition rate, roughness (Ra), hardness (H), elastic modulus (E), resistance to plastic deformation (H_3/E_2) and critical load (L_C) of TiAlN coatings. The low roughness obtained can be attributed to the achieved surface finish of substrates and deposition parameters, including pressure, bias and temperature [21], [28].

TABLE IV: Characteristics of the TiAlN coatings

Thickness (nm)	535 ± 12
Deposition rate (nm.min^{-1})	4.5
Ra (nm)	43.3 ± 4.8
H (GPa)	26.8 ± 3.9
E (GPa)	420.1 ± 20.3
H^3/E^2	0.1094 ± 0.034
L_C (N)	34 ± 3

Investigations indicate that the mechanical properties of ternary Ti based compounds are related to the amount of substitutional atoms in the fcc-TiN structure. In TiAlN coatings, with aluminum addition below 70%, a NaCl-type structure is maintained while the hardness is increased with aluminum content. For higher aluminum additions, hardness decreases due to the change in crystalline structure from NaCl to wurtzite ZnS (i.e. AlN) [29], [30]. In the present work, the analysis of representative EDS showed an aluminum atomic percentage near to 40%, explaining the higher hardness of TiAlN coating as well as the resistance to plastic deformation compared with the mechanical properties of TiN coatings (H = 16.9 ± 1.9 GPa and H^3/E^2 = 0.058 ± 0.008) as previously reported [31].

B. Coefficient of friction

Figure 2 shows the coefficient of friction of TiAlN thin films as a function of the number of sliding cycles for different counterparts and applied loads. Figure 2a shows that, for the lower applied load, the TiAlN coupled against 100Cr6 has exhibited the highest and unstable COF along the entire test. This behavior was attributed to a combination of factors, such as the initial contact area, the chemical reactivity of the contacting surfaces and the debris formation.

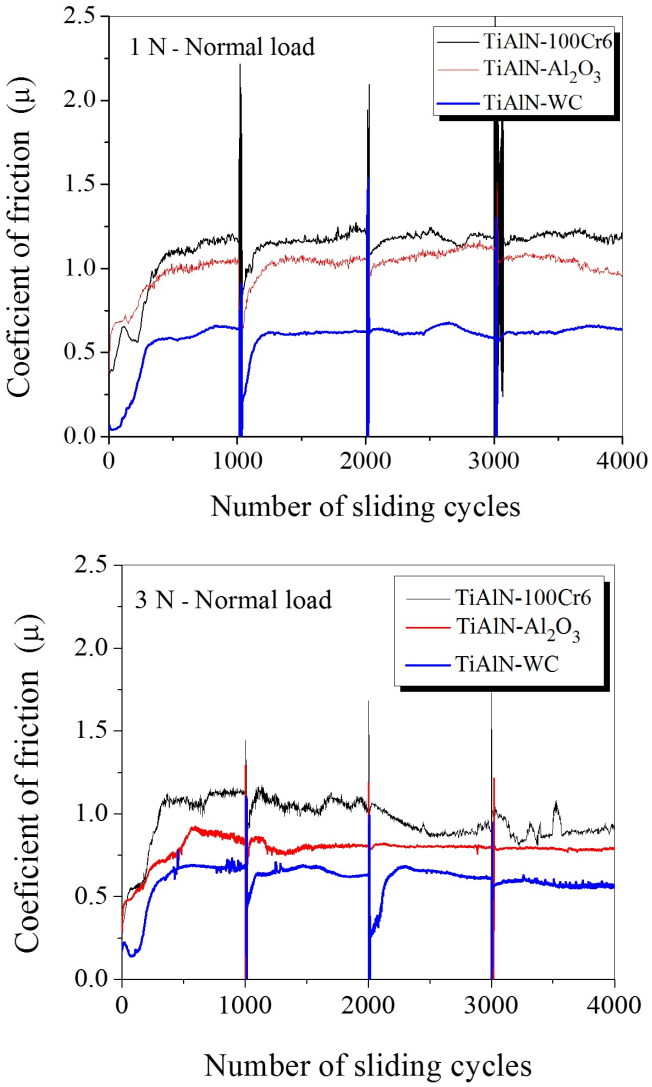

Fig. 2: Coefficient of friction for TiAlN coating sliding against different counterparts for normal loads of 1 N (a) and 3 N (b).

As it can be seen in Table V, when the softest counterpart 100Cr6 was slid against the TiAlN coating, the highest initial contact area and consequently, the lowest Hertzian stresses were generated (Eq. 2). The behavior of COF for the TiAlN-100Cr6 pair was also influenced by the metallic nature of 100Cr6 counterpart, which tends to produce fragile oxidation products with high and unstable friction [32]. Previous chemical studies of the wear track have shown the formation of mixed Fe and Al oxides, that promotes oxidative and abrasive wear mechanisms (ploughing) [32], [33]. The instability in COF during the first 1000 cycles was

also influenced by wear particles (debris) ejected from the ball contact surface and generated from wearing of asperities peaks. Between 2000 and 3000 cycles, variations in COF were observed caused by morphologic changes in the wear track, leading to the formation of new plastically deformed debris, as will be shown later. The average value and variations in COF for the TiAlN coating against Al_2O_3 were slightly lower than the metallic counterpart. This behavior was related to the higher hardness and the lower reactivity of the Al_2O_3 counterpart, which produced a lower contact area and a higher Hertzian stress, compared with the TiAlN-100Cr6 pair [21], [33]. The same coating tested against WC-Co showed the lowest fluctuations and average COF approximately two times lower than that with 100Cr6 counterpart. In this case, the TiAlN coating slid against the hardest counterpart, which led to the smallest contact area and the highest Hertzian stress. The debris originated from this sliding pair may be smaller and the reactivity of the contact surface may result in more lubricious products.

TABLE V: Mechanical properties and initial maximum Hertzian stress for the used counterpart

Counterpart characteristics			Maximum Hertzian stress (GPa)	
Counterpart (ball)	Hardness (GPa)	Elastic modulus (GPa)	Normal load (N)	
			1 N	3 N
100Cr6	8.5	210.3	0.79	1.14
Al_2O_3	13.5	370.4	0.97	1.40
WC	22.2	630.2	1.14	1.65

Certain tendency is observed in the friction behavior of the studied pairs, pointing that, increasing the hardness and decreasing the reactivity of the counterpart increase the time to reach a steady state friction. Additionally, a harder and less reactive counterface lead to a lower average and a more stable coefficient of friction.

The increase in the applied load increased the Hertzian stress, as seen in Table V. Higher contact stress induces fatigue, producing premature coating failure and debris formation [15]. For 100Cr6 counterpart, elevated instabilities in the COF were observed during the whole test run with 3 N of applied load. After 2000 cycles, the COF decreases, probably due to coating delamination and substrate debris presence in the wear track.

C. Wear coefficient

Figure 3 shows the evolution of wear coefficient for TiAlN coatings sliding against the different counterparts every 1000 cycles. For sliding tests conducted with a load of 1 N, a lower wear coefficient was obtained, which was also related to the lower Hertzian stress (Table V). With 3 N, a higher contact pressure produces a higher coating/substrate deflection, increasing wear by coating delamination and debris formation.

The wear coefficient of TiAlN-100Cr6 tribopair in both loads was superior to the other counterpairs. Lower mechanical properties of 100Cr6 counterpart produce higher contact area, promoting material transference and oxidative and abrasive wear mechanisms. With ceramic counterparts, superior mechanical properties produce lower contact area but superior Hertzian stress with wear concentration in the middle of the wear track. However, the chemical stability of ceramic counterparts produces protective debris that contributes with the load support, reducing the wear coefficient.

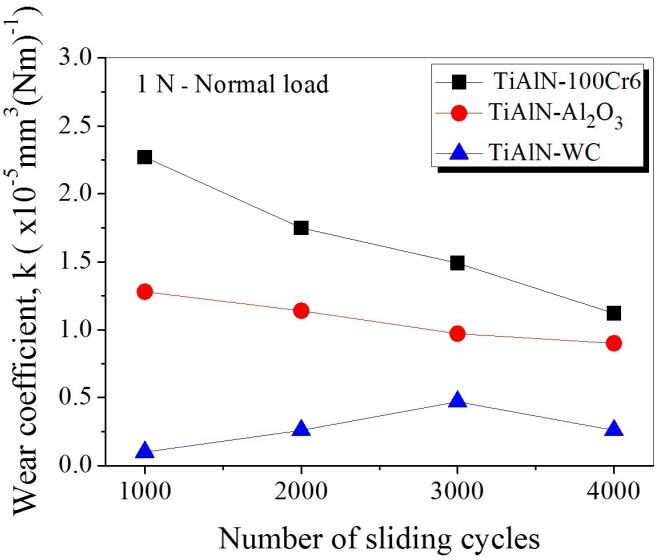

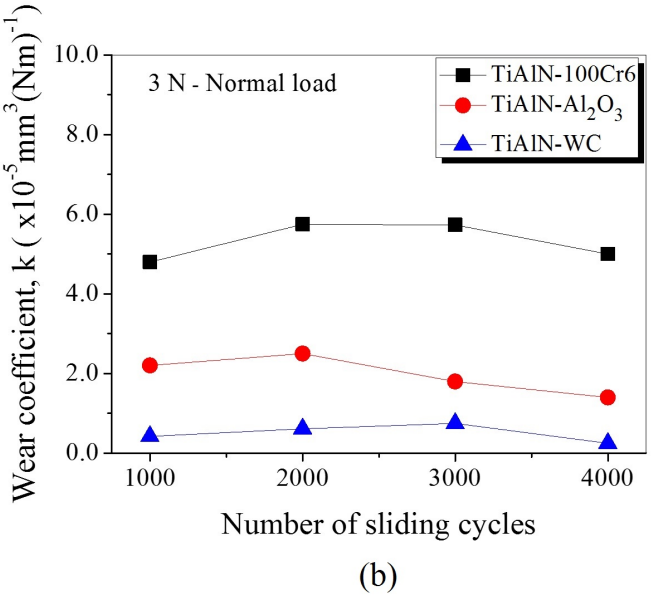

Fig. 3: Wear coefficients of TiAlN thin films sliding against different counterparts with (a) 1 N and (b) 3 N of applied load.

D. Worn surfaces

The roughness profiles obtained from the wear tracks in all the sliding conditions (counterpair and applied load) are shown in Figure 4 and Figure 5. Table VI also shows the principal results of the present study, including a counterpart (ball) hardness to the coating hardness ratio or relative hardness (H_b/H_f), average coefficient of friction, wear coefficient and track width.

Wear profiles obtained by profilometry (Figure 4) showed that a decrease in the ball hardness caused an increase in the track width. According to Figure 4a, the wear of TiAlN against 100Cr6 was severe even in the initial stages (1000 cycles) of the sliding test. Wear profiles of TiAlN coating sliding against

TABLE VI: Relative hardness (H_b/H_f), friction and wear results of the contacting pairs

Counterpart	H_b/H_f	Average coefficient of friction, μ		Wear coefficient, k (x10^{-5}mm^3(Nm)$^{-1}$)		Track width (μm)	
		1 N	3 N	1 N	3 N	1 N	3 N
100Cr6	0.32	1.20	0.90	1.10	5.00	370	463
Al2O3	0.50	1.10	0.80	0.90	1.10	261	293
WC	0.83	0.61	0.58	0.25	0.30	194	286

the Al_2O_3 ball (Figure 4b) showed a progressive increase in both the depth and width of the wear track as the number of sliding cycles was increased. In the final stages of the test, wear depth overcame the coating only in some sectors of the track. When the WC counterpart was used, the roughness profiles measurements (Figure 4c) indicated a lower wear of the TiAlN coating.

A higher applied load of 3 N produced an increase in the depth and width of the wear track (Figure 5), which is a confirmation of the increase in the wear coefficient, as showed in Figure 3 (see also Table VI). These effects were more significant for the metallic counterpart. The hills that can be observed in all the wear profiles might be an indication of the presence of a third body in the wear tracks, due to the plastic deformation, material transference and welding of some of the fragments that were detached and entrapped in the sliding contact area. These characteristics were confirmed by the analysis of micrographs and the chemical composition of wear tracks, as will be shown below.

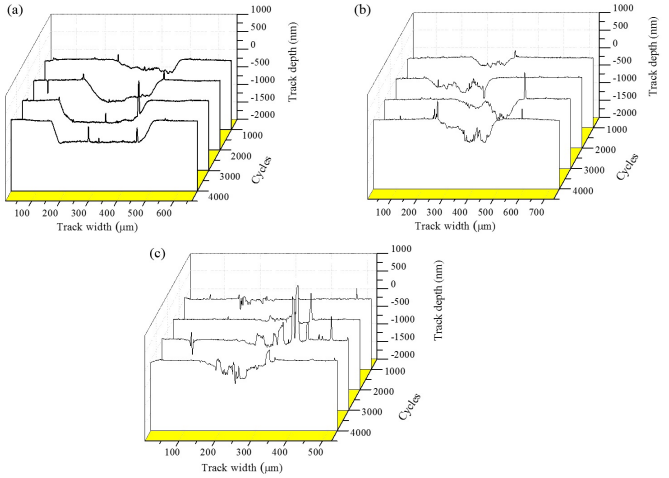

Fig. 4: Wear profiles taken every 1000 cycles for the different counterparts. Test parameters: 1 N, 10 cm.s^{-1}. Counterparts: (a) 100Cr6, (b) Al_2O_3 and (c) WC.

Figure 6 shows 100X micrographs of wear scars for TiAlN coating after 4000 cycles under the normal loads 1 N and 3 N. When the 100Cr6 counterpart was used in a sliding test with a normal load of 1 N, an adhesive failure of the TiAlN coating was observed, seen that large coating regions were detached from the substrate through spalling (Figure 6a).This explain the smooth wear track profiles showed above (Figure 4a). Granular debris and transferred material were also observed, probably, being a mixture of iron and chromium (from the 100Cr6 counterpart), iron (from the steel substrate) and titanium-aluminum-containing oxides (from the film). Higher normal load levels of 3 N have intensified the occurrence of tribochemical reaction, since almost all the wear track was covered by the oxide tribolayer that could be formed as a result of the reaction of the chromium-containing bearing material against the TiAlN coating. This explains the highest peaks in the wear track profiles and the width of the wear track (Figure 5a).

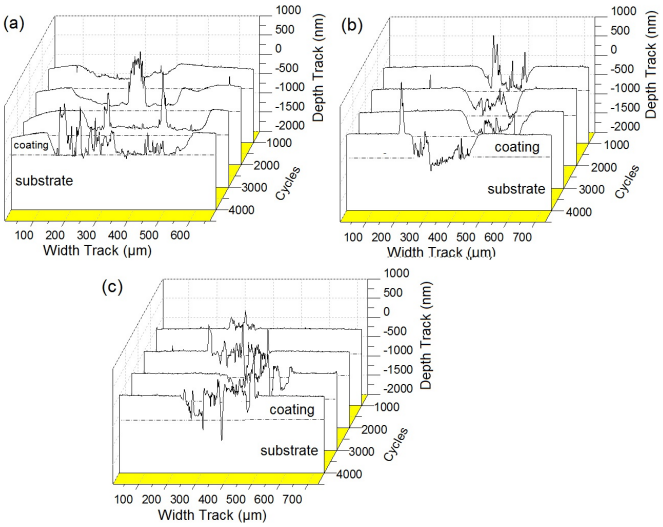

Fig. 5: Wear profiles taken every 1000 cycles for different counterparts. Test parameters: 3 N, 10 cm.s^{-1}. Counterparts: (a) 100Cr6, (b) Al_2O_3 and (c) WC.

Similar adhesive failure of the TiAlN coating was observed after 4000 sliding cycles against the Al_2O_3 counterface (Figure 6b), compared to the TiAlN-100Cr6 sliding pair, but the material transfer and the oxidation phenomena were less intense. The increase in normal load also increased the amount of lost particles accumulated at the edge of the wear track and also, intensified the tribochemical reaction by the formation of a tribolayer probably consisting of iron oxide (from the substrate) and Ti and Al oxide (from the film and the counterface). However, compared with TiAlN-100Cr6 pair, the amount of oxide products was lower, which can be attributed to the lower reactivity of the Al_2O_3 counterface [21] and also explains the lower wear coefficient (Figure 3) of this sliding pair. In the case of the TiAlN-WC sliding pair, the wear mechanism appeared predominantly by a tribochemical reaction and the adhesive failure of the film was concentrated in the middle of the wear track where the contact pressure reaches a maximum (Figure 6c). The less substrate exposure explains the characteristics of the wear profiles (Figure 4c and Figure 5c) and the lowest values of wear coefficient (3) for this sliding pair. In accordance, the tribolayer may be composed of a mixture of tungsten oxide (from the counterface) and Ti-Al oxide (from the film), which offered the best tribology

behavior, i.e., the lowest values of wear coefficient and friction coefficient between the three sliding pairs studied in this work.

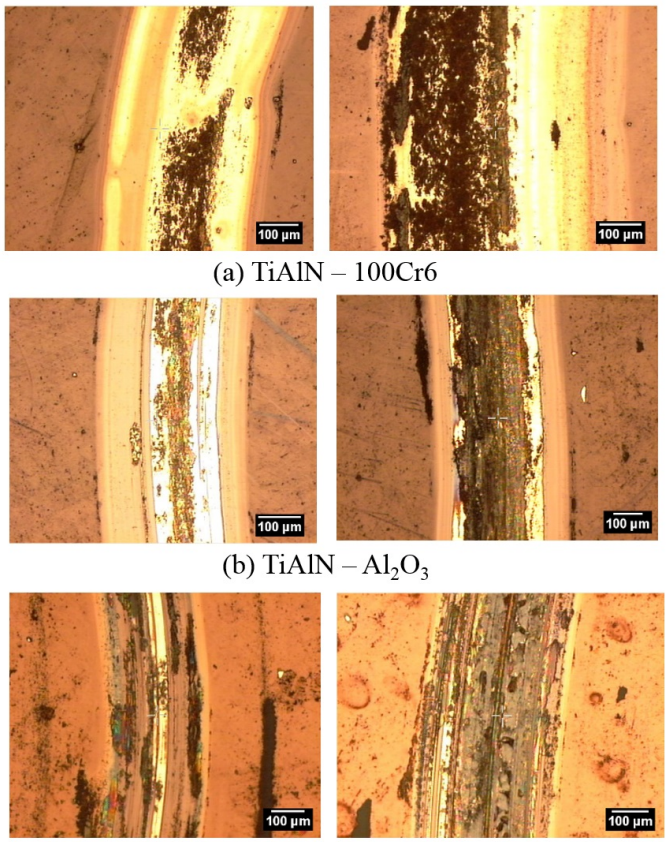

(a) TiAlN – 100Cr6

(b) TiAlN – Al_2O_3

(c) TiAlN – WC

Fig. 6: Micrographs (100X) of the wear track for the TiAlN coating sliding against (a) 100Cr6, (b) Al_2O_3 and (c) WC counterparts under normal loads of 1 N and 3 N.

SEM and EDS superficial elemental mapping images from the wear track obtained under 1 N of normal load are shown in Figure 7. SEM analyses (Figure 7a,b) confirmed that the wear track of the TiAlN coating was covered by a tribolayer, formed on the sliding contact areas by mixing the detached particles from both the coating and Al_2O_3 counterpart. Through the EDS analyses (Figure 7c), it was also verified that the tribolayer has contained oxygen, due to the coating oxidation by the frictional heat promoting TiO_2 and Al_2O_3 formation [21], [32]. Furthermore, this oxygen-rich tribomaterial was subsequently deformed by the contact pressure, fragmented and finally detached to form the wear particles (Figure 7c). Thus, fatigue produced crack nucleation and propagation, generating new debris (Figure 7c), some of which mechanically mixed by the action of shear and compressive stresses to form the tribolayer while others were hardened and became a large abrasive, producing the groves in the center of the wear track (Figure 7a) [14].

The results of this work indicated that the chemical nature and the mechanical properties of the counterpairs contribute with the tribological characteristics of wear particles and the oxide-containing tribolayer, during the sliding contact, and have played an important role in determining both the wear coefficient and the frictional levels of the sliding pairs (Figure 7 and Figure 8).

During the sliding, coating detached particles are transformed into TiO_2 and Al_2O_3 oxides (Eq. 6). These oxides have hydrophilic properties with a capability to absorb water molecules from the atmosphere favoring hydrated oxides formation like $Al(OH)_3$, the most chemically stable (Eq.7) [33]–[35].

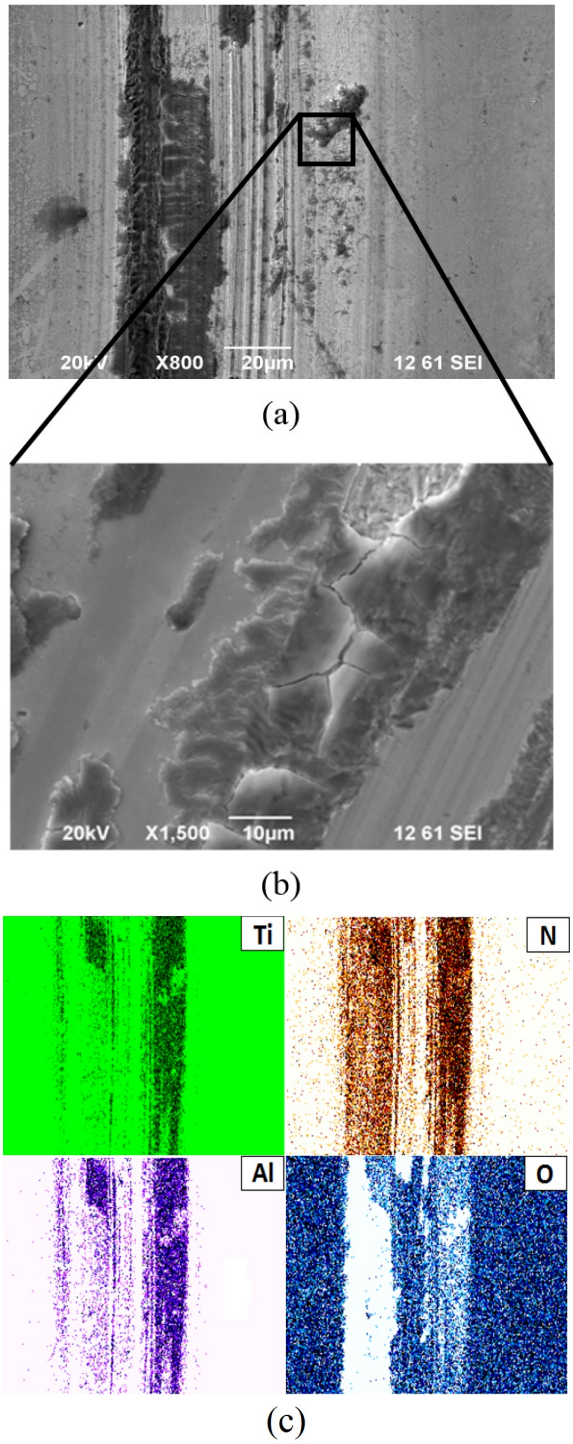

Fig. 7: SEM morphologies, EDS and elemental composition of the TiAlN wear track. (a) 800X superficial SEM of the wear track, (b) 1500X amplification of a welded, plastically deformed particle and (c) superficial elemental EDS mapping (the darkest areas indicate a lower content of the element).

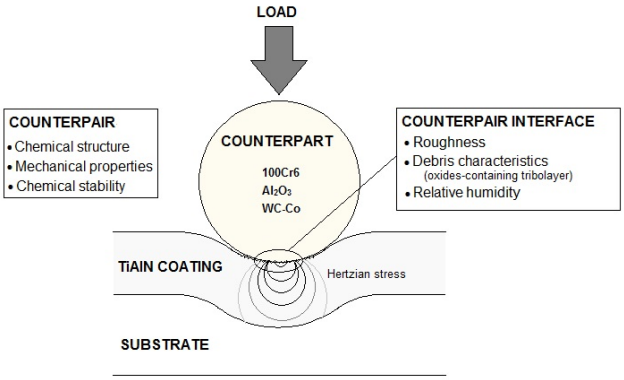

Fig. 8: Simplified schematic representation of counterpairs sliding contact.

$$4TiAlN(coating) + 7O_2 \rightarrow 4TiO_2 + 2Al_2O_3 + 2N_2 \quad (6)$$

$$Al_2O_3 + 3H_2O \rightarrow 2Al(OH)_3 \quad (7)$$

The counterpart hardness to coating hardness ratio (H_b/H_f), was also used for analyzing the effect of counterpart particles transference and the possible tribomaterial formation and their correlation with the intensities of the wear coefficient and coefficient of friction (Table VI).

In particular, the highest values of wear coefficient for the TiAlN-100Cr6 pair were considered to be due to lower relative hardness of 100Cr6 counterpair (H_b/H_f = 0.32) which was easily cracked to form small fragments by the action of the normal and shear stresses developed at the sliding contact. The fragments of 100Cr6 counterpart were transformed into chromium oxide (Cr_2O_3) and iron oxide (Fe_2O_3) mainly, and transferred to TiAlN coating surface. Iron oxide also was formed by the substrate exposure due to the coating spalling damage. These mechanically mixed oxides have a high shearing resistance producing a high level of friction [35], [36]. Moreover, this iron oxide-containing tribomaterial is easy to separate and fracture from the contacting surface due to its low cohesion and ductility leading to an intense coating spalling, oxidative wear and abrasive wear.

Due to higher relative hardness (H_b/H_f = 0.50), lower chemical reactivity and ionic-bonding, the Al_2O_3 ball was less prompt to crack and to chemical transformation. Thus, the TiAlN coating sliding against the Al_2O_33 counterpart has exhibited coating damage by spalling as well as oxidative and abrasive wear mechanisms in a lower intensity, i.e., the TiAlN coating showed a lower wear coefficient. The mixed oxide tribolayer is composed of Al_2O_3, TiO_2 protective oxides and a lower iron oxide presence compared with the 100Cr6 counterpart due to lower wear track depth, which produced a slight decrease in friction.

The WC-Co counterpart has the highest relative hardness (H_b/H_f = 0.83), that contributes with lower material transference. Compared with Al_2O_3 counterpart which is chemically inert, the WC-Co counterpart is chemically reactive and can present oxidation in high-oxygen atmosphere. The EDS representative analysis of tribolayer shows that it contain Ti, Al, W, C, Co, O and N. The Fe and Cr presence is believed to be due to substrate (Table VII).

TABLE VII: The element composition of the TiAlN/WC-Co interface

Element	At. %
Ti	9.42 ± 0.09
Al	4.17 ± 0.03
N	1.60 ± 0.35
Fe	24.10 ± 0.07
C	5.70 ± 0.21
Cr	10.28 ± 0.03
W	5.49 ± 0.02
Co	1.03 ± 0.05
O	38.21 ± 0.17
Total	100.00

According to the composition detected, the wear track consists possibly of WC and Co counterpart particles as well as of WO_3, $CoWO_4$, Al_2O_3 and TiO_2 oxides with high cohesion and ductility [34], [37], [38]. The presence of $CoWO_4$ and WO_3 in the tribolayer can be related to the higher-oxygen presence by the hydrophilic capability of TiO_2 and Al_2O_3. According to the literature, tungsten-containing oxides have a low shearing resistance and, hence, a high lubricity, which is consistent with the lowest values of friction coefficient of the TiAlN-WC pair [35], [38].

IV. Conclusões

For the unidirectional sliding dry tests of TiAlN coating against various counterpart materials, the normal load as well as the hardness and the chemical reactivity of the counterface affect the characteristics of the tribomaterial, the friction and wear behavior of the TiAlN coating.

- The increase in normal load from 1 N to 3 N increases both the average value and the instability of the coefficient of friction, in spite of the dissimilar composition and the hardness of the counterpart.
- The wear coefficient of the TiAlN coating also increases with the higher load level due to superior coating/substrate deflection, which increases the wear by coating delamination and debris formation.
- The coating wear behavior when using 100Cr6 metallic counterpart is characterized by a tribochemical reaction involving oxidation of the coating and oxidation of the transferred counterface detached particles. Abrasion wear and adhesive failure through spalling of the coating also occur by the action of the hardened mechanically mixed abrasive particles.
- Higher mechanical properties of Al_2O_3 and WC-Co ceramic counterparts produce superior Hertzian stress as well as lower contact area promoting a coating wear, mainly in the middle of the wear track. The lower coating wear is explained by the lower material transference and the protective debris formation, which act as a third body with load-support capability.
- The lowest wear coefficient and coefficient of friction of coating sliding against WC-Co counterpart is related to the highest relative hardness (H_b/H_f), as well as to the formation of a tribofilm composed of mixed oxides with low shearing stress and high lubricity.

ACKNOWLEDGEMENTS

The authors thank partial support of this work from Laboratorio de Recubrimientos Duros y Aplicaciones Industriales (RDAI).

V. REFERENCES

[1] M. Soković, B. Barišić, and S. Sladić, "Model of quality management of hard coatings on ceramic cutting tools," *Journal of Materials Processing Technology*, vol. 209, no. 8, pp. 4207 – 4216, 2009.

[2] G.S. Fox-Rabinovich, A.I. Kovalev, M.H. Aguirre, B.D. Beake, K. Yamamoto, S.C. Veldhuis, J.L. Endrino, D.L. Wainstein, and A.Y. Rashkovskiy, "Design and performance of altin and TiAlCrN PVD coatings for machining of hard to cut materials," *Surface and Coatings Technology*, vol. 204, no. 4, pp. 489 – 496, 2009.

[3] C Mitterer, F Holler, F Üstel, and D Heim, "Application of hard coatings in aluminium die casting — soldering, erosion and thermal fatigue behaviour," *Surface and Coatings Technology*, vol. 125, no. 1–3, pp. 233 – 239, 2000.

[4] Vipin Chawla, R. Jayaganthan, and Ramesh Chandra, "Structural characterizations of magnetron sputtered nanocrystalline TiN thin films," *Materials Characterization*, vol. 59, no. 8, pp. 1015 – 1020, 2008.

[5] Wen-Jun Chou, Ge-Ping Yu, and Jia-Hong Huang, "Mechanical properties of TiN thin film coatings on 304 stainless steel substrates," *Surface and Coatings Technology*, vol. 149, no. 1, pp. 7 – 13, 2002.

[6] Sa-Kyun Rha, Won-Jun Lee, Seung-Yun Lee, Yong-Sup Hwang, Yoon-Jik Lee, Dong-Il Kim, Dong-Won Kim, Soung-Soon Chun, and Chong-Ook Park, "Improved TiN film as a diffusion barrier between copper and silicon," *Thin Solid Films*, vol. 320, no. 1, pp. 134 – 140, 1998.

[7] O. Knotek, M. Boehmer, and T. Leyendecker, "On structure and properties of sputtered ti and al based hard compound films," *Journal of Vacuum Science & Technology, A; (United States)*, vol. 4:6, Nov 1986.

[8] Wolf-Dieter Münz, "Titanium aluminum nitride films: A new alternative to TiN coatings," *Journal of Vacuum Science & Technology A*, vol. 4, no. 6, pp. 2717–2725, 1986.

[9] Li Chen, Martin Moser, Yong Du, and Paul H. Mayrhofer, "Compositional and structural evolution of sputtered Ti-Al-N," *Thin Solid Films*, vol. 517, no. 24, pp. 6635 – 6641, 2009.

[10] Paul H. Mayrhofer, Christian Mitterer, Lars Hultman, and Helmut Clemens, "Microstructural design of hard coatings," *Progress in Materials Science*, vol. 51, no. 8, pp. 1032 – 1114, 2006.

[11] Li Chen, Yong Du, She. Q. Wang, Ai. J. Wang, and H.H. Xu, "Mechanical properties and microstructural evolution of tin coatings alloyed with al and si," *Materials Science and Engineering: A*, vol. 502, no. 1–2, pp. 139 – 143, 2009.

[12] J.Y. Rauch, C. Rousselot, and N. Martin, "Structure and composition of $tixal1-xn$ thin films sputter deposited using a composite metallic target," *Surface and Coatings Technology*, vol. 157, no. 2–3, pp. 138 – 143, 2002.

[13] I.J. Smith, D. Gillibrand, J.S. Brooks, W.-D. Münz, S. Harvey, and R. Goodwin, "Dry cutting performance of HSS twist drills coated with improved tialn," *Surface and Coatings Technology*, vol. 90, no. 1–2, pp. 164 – 171, 1997.

[14] J.L. Mo and M.H. Zhu, "Tribological oxidation behaviour of PVD hard coatings," *Tribology International*, vol. 42, no. 11–12, pp. 1758 – 1764, 2009, Special Issue: 35th Leeds-Lyon Symposium.

[15] Kenneth Holmberg, Allan Matthews, and Helena Ronkainen, "Coatings tribology—contact mechanisms and surface design," *Tribology International*, vol. 31, no. 1–3, pp. 107 – 120, 1998.

[16] D. McIntyre, J.E. Greene, G. Hakansson, J.-E. Sundgren, and W.D.Münz, "Oxidation of metastable single-phase polycrystalline Ti0.5Al0.5N films: kinetics and mechanisms," *Journal of Applied Physics*, 1990.

[17] L Hultman, "Thermal stability of nitride thin films," *Vacuum*, vol. 57, no. 1, pp. 1 – 30, 2000.

[18] T.E Fischer, Z Zhu, H Kim, and D.S Shin, "Genesis and role of wear debris in sliding wear of ceramics," *Wear*, vol. 245, no. 1–2, pp. 53 – 60, 2000.

[19] Huiwen Liu and Qunji Xue, "Wear mechanisms of zirconia/steel reciprocating sliding couple under water lubrication," *Wear*, vol. 201, no. 1–2, pp. 51 – 57, 1996.

[20] Z. Zhou, W.M. Rainforth, C.C. Tan, P. Zeng, J.J. Ojeda, M.E. Romero-Gonzalez, and P.Eh. Hovsepian, "The role of the tribofilm and roll-like debris in the wear of nanoscale nitride PVD coatings," *Wear*, vol. 263, no. 7–12, pp. 1328 – 1334, 2007, 16th International Conference on Wear of Materials.

[21] M.F. Cano, J.S. Restrepo, A. Ruden, J. M. González, and F. Sequeda, "The effect of substrate temperatures on tribological behavior of Ti-Al-N coating deposited by magnetron sputtering," in *52th SVC Technical Conference Proceedings*, 2009, pp. 601–607.

[22] A. Ruden, J. M. Gonzalez, J.S. Retrepo, M.F. Cano, and F. Sequeda, "Tribology of ZrN, CrN and TiAlN thin films deposited by reactive magnetron sputtering," *Dyna*, vol. 80, no. 178, pp. 95–100, 2013.

[23] W.C Oliver and G.M. Pharr, "An improved technique for determining hardness and elastic modulus using load and displacement sensing indentation experiments," *Journal of Materials Research*, vol. 7, no. 6, pp. 1564–1583, 1992.

[24] J. Chen and S.J. Bull, "Invited review," *Vacuum*, vol. 83, no. 6, pp. 911–920, 2009.

[25] A Leyland and A Matthews, "On the significance of the H/E ratio in wear control: a nanocomposite coating approach to optimised tribological behaviour," *Wear*, vol. 246, no. 1–2, pp. 1 – 11, 2000.

[26] J.F. Archard and W. Hirst, "The wear of metals under unlubricated conditions.," *Proceedings of the Royal Society of London*, vol. A236, pp. 397–410, 1956.

[27] Hong-Ying Chen, Jui-Hong Chen, and Fu-Hsing Lu, "Evaluation of poisson's ratio and young's modulus of nitride films by combining grazing incidence X-ray diffraction and laser curvature techniques," *Thin Solid Films*, vol. 516, no. 2–4, pp. 345 – 348, 2007.

[28] J.T. Chen, J. Wang, F. Zhang, G.A. Zhang, X.Y. Fan, Z.G. Wu, and P.X. Yan, "Characterization and temperature controlling property of TiAlN coatings deposited by reactive magnetron co-sputtering," *Journal of Alloys and Compounds*, vol. 472, no. 1–2, pp. 91 – 96, 2009.

[29] F. Quesada, A. Mariño, and E. Restrepo, "Tialn coatings deposited by r.f. magnetron sputtering on previously treated {ASTM} {A36} steel," *Surface and Coatings Technology*, vol. 201, no. 6, pp. 2925 – 2929, 2006.

[30] S. PalDey and S.C. Deevi, "Single layer and multilayer wear resistant coatings of (Ti,Al)N: a review," *Materials Science & Engineering A*, vol. 342, no. 1-2, pp. 58 – 79, 2003.

[31] G. A. Holguín, M. F. Cano, A. Ruden, J. M. González, P.A. Jurado, and F. Sequeda, "Estudio de las propiedades mecánicas, tribologícas y superficiales de recubrimientos duros basados en titanio," *Revista Latinoamericana de Metalurgia y Materiales*, vol. 33, pp. 1 – 10, 2013.

[32] K. Singh, P.K. Limaye, N.L. Soni, A.K. Grover, R.G. Agrawal, and A.K. Suri, "Wear studies of (Ti-Al)N coatings deposited by reactive magnetron sputtering," *Wear*, vol. 258, no. 11-12, pp. 1813–1824, 2005, cited By 26.

[33] M.A. AL-Bukhaiti, K.A. Al-hatab, W. Tillmann, F. Hoffmann, and T. Sprute, "Tribological and mechanical properties of Ti/TiAlN/TiAlCN nanoscale multilayer PVD coatings deposited on AISI H11 hot work tool steel," *Applied Surface Science*, vol. 318, pp. 180 – 190, 2014, NANOTR9, 9th Nanoscience and Nanotechnology Conference Special Issue.

[34] Xin Wang, Parick Y. Kwon, David Schrock, and Dave (Dae-Wook) Kim, "Friction coefficient and sliding wear of altin coating under various lubrication conditions," *Wear*, vol. 304, no. 1–2, pp. 67 – 76, 2013.

[35] Ali Erdemir, "A crystal-chemical approach to lubrication by solid oxides," vol. 8, no. 2-3, pp. 97–102+, 2000.

[36] A. Öztürk, K.V. Ezirmik, K. Kazmanlı, M. Ürgen, O.L. Eryılmaz, and A. Erdemir, "Comparative tribological behaviors of TiN, CrN and MoNCu nanocomposite coatings," *Tribology International*, vol. 41, no. 1, pp. 49 – 59, 2008.

[37] S Descartes and Y Berthier, "Rheology and flows of solid third bodies: background and application to an $MoS_1.6$ coating," *Wear*, vol. 252, no. 7–8, pp. 546 – 556, 2002.

[38] S.N. Basu and V.K. Sarin, "Oxidation behavior of WC-Co," *Materials Science and Engineering: A*, vol. 209, no. 1–2, pp. 206 – 212, 1996, Proceedings of the 5th International Conference on the Science of Hard Materials.